Rates and Mechanisms of Conversion of Ice Nanocrystals to Ether Clathrate Hydrates: Guest-Molecule Catalytic Effects at ∼120 K

Dheeraj B. Gulluru and J. Paul Devlin*

Department of Chemistry, Oklahoma State University, Stillwater, Oklahoma 74078

Received: October 30, 2005; In Final Form: December 8, 2005

A Fourier transform infrared investigation of the rates and energetics of conversion of ice nanocrystals within 3-D arrays to ether clathrate−hydrate (CH) particles at ∼120 K is reported. After an induction period, apparently necessitated by relatively slow nucleation of the CH phase, the well-established shrinking-core model of particle−adsorbate reaction applies to these conversions in the presence of an abundance of adsorbed ether. This implies that the transport of the ether adsorbate through the product crust encasing a reacting particle core (a necessary aspect of a particle reaction mechanism) is the rate-controlling factor. Diffusion moves adsorbed reactant molecules to the reaction zone at the interface of the ice core with the product (CH) crust. The results indicate that ether hydrate formation rates near 120 K resemble rates for gas hydrates measured near 260 K, implying rates greater by many orders of magnitude for comparable temperatures. A surprising secondary enhancement of ether CH-formation rates by the simultaneous incorporation of simple small gas molecules (N_2, CO_2, CH_4, CO, and N_2O) has also been quantified in this study. The rapid CH formation at low temperatures is conjectured to derive from defect-facilitated transport of reactants to an interfacial reaction zone, with the defect populations enhanced through transient H bonding of guest−ether proton-acceptor groups with O−H groups of the hydrate cage walls.

1. Introduction

Clathrate−hydrate formation/decomposition is of both fundamental and practical interest.[1−5] The practical interest stems primarily from the great abundance of CHs on earth (and presumably elsewhere) and the potential commercial value and societal danger represented by their presence. There exist (e.g., on the floor of the oceans) methane deposits adequate to fuel society for a considerable time and sufficient CH_4 and CO_2 deposits to suggest a threat to civilization should they be released.[6] Our more basic interests derive from the ability of moderately good proton-acceptor molecules, such as ethers, formaldehyde,[7] and acetone,[8] to form crystalline clathrate hydrates at remarkably low temperatures. We showed in the past that the ether CHs can be formed by several methods at ∼120 K: direct vapor deposition of the proper mixtures,[9] by warming an appropriate amorphous solid mixture,[10] as particles condensed in cold cluster cells[11] and by vapor interaction with ice nanocrystals.[12] This ability, of the complex crystal structures of the classic structure I and structure II CHs, with unit cells of 46 and 136 water molecules,[13] to organize at temperatures well below the minimum temperature at which crystalline ice (of relatively simple structure) can normally be deposited is impressive.

Here, we seek increased understanding of this low-temperature formation of CHs of proton-acceptor guest molecules using a different approach: the determination of the transport rates and associated activation energies by which the ether guest molecules move through the condensed phase during conversion of ice nanocrystals to nanocrystals of the CHs. Most CHs, including those of CO_2 and CH_4, will not form extensively in the absence of high pressures and temperatures > 200 K. These are the conditions used recently by Wang et al. in novel kinetic measurements of the formation rates of CHs of CO_2 and CH_4 as monitored by neutron diffraction.[1,14] Their results established that, for gas pressures of ∼1000 psi and temperatures near 270 K, conversion of micrometer-sized ice particles (i.e., <250 μm) to CHs occurs over many hours at rates controlled by the diffusion of the guest molecules through the growing crust of CH. This conclusion parallels ours from kinetic studies of formation of ammonia- and acid-hydrate nanoparticles from ice nanocrystals in the 100−130 K range.[15−17] We will see below that rate variation with time for conversion of ice nanocrystals to clathrate hydrates can be quite different than observed for acid- and ammonia-hydrate formation reactions. Nevertheless, as for formation of the acid/base hydrates and the CO_2 and CH_4 CHs, the rate-controlling process throughout much of the nanoparticle conversion is identified with transport of the guest molecules through the product (CH) crust to the reaction zone at the ice−product interface. That is, CH formation, like acid hydrate formation at these low temperatures,[17] can be viewed as a solid-phase reaction unrelated to diffusion/dissolution of isolated molecules in *ice.* Further, the temperature appropriate for kinetic observations of ether CH formation on a laboratory time scale lies within the range reported for acid-hydrate formation; i.e., from 112 to 135 K or more than 140 K below that used in the gas-hydrate kinetic studies.[1,14]

This remarkable CH-formation capacity of proton-acceptor guest molecules has been related to an unusual orientational mobility induced in the CH host network.[18−21] The CHs of small ether molecules (tetrahydrofuran (THF), dimethyl ether (DME), ethylene oxide, and trimethylene oxide), along with a few other proton-acceptor guest molecules, have remarkably high dielectric-relaxation rates, several orders of magnitude greater than ice or more typical CHs.[13,20,22] This unusual mobility is thought to derive from the injection of orientational defects into the icelike

* To whom correspondence should be addressed. E-mail: devlin@okstate.edu.

10.1021/jp056254u CCC: $33.50
Published on Web 01/11/2006

host structure following transient coordination of the proton acceptors with the OH bonds of the CH cage walls.[18,20] The exceptional mobility is further reflected in an unusual isotopic exchange rate within the CH of ethylene oxide.[19] Clathrate hydrate neighbor-coupled HDO units were observed to move apart at temperatures below 90 K at the rate observed for crystalline ice near 140 K.[23]

2. Experimental Methods

The kinetic studies of the conversion of ice nanocrystals to hydrate nanoparticles have followed the development of methods to prepare 3-D arrays of nanocrystals of cubic ice.[24] Such arrays assemble naturally on surfaces within double-walled cold collisional-cooling cells in which ice aerosols are prepared. For example, 3-D arrays of ~20 nm average diameter ice crystals form when ~1.5% mixtures of water in helium are rapidly expanded into a cell held near 110 K.[25] At this temperature, ~4% of the ice aerosol particles that form become attached to the two ZnS end windows of the inner cell chamber. The thickness of an array can be controlled by multiple loading and pump cycles so that samples are obtained with an optical density that is optimum for Fourier transform infrared (FTIR) transmission spectroscopic measurements. Then, the FTIR spectra allow ready identification and quantification of the ice and of hydrates that form during reaction with the ice.

The CH formation temperatures used in this kinetic study were generally in the 114−126 K range. Typically, ~20-nm particles (average diameter) of ice in a 3-D array were prepared at 110 K. On the basis of the intensity of the dangling-hydrogen mode at 3692 cm^{-1} the average size of such particles changes only marginally upon warming to temperatures between 114 and 126 K. An abundance of ether molecules available for reaction was provided by embedding ether particles within the ice arrays by alternately charging the particle cell with water and ether mixes in He(g) during preparation of an ice array. The volatility of the embedded ether particles (for the small ethers studied, namely, ethylene oxide (EO), DME, and THF) was ample to provide the necessary abundance of reactant ether guest molecules at the ice-particle surfaces. Once formed, the particle arrays were warmed rapidly to the ice-to-CH-conversion temperature, which was chosen so that only a small fraction of ice reacted before the initiation of rate measurements at the target temperature. As the data will show (section 3) the amount of reaction prior to establishment of the reaction temperature was also limited by an induction period apparently related to nucleation of the CH phase.

The CHs of this study each have well-known IR spectra that provide a choice of bands for monitoring the extent of reaction.[9−11] However, the quantitative measurement of the amount of ice transformed to CH was determined by evaluating the fraction of converted ice through comparison of the sample O−H stretch spectrum with the initial spectrum of the bare ice nanoparticles (as in Figure 1) using FTIR differencing methods. After reaction rates were established for formation of the simple CHs of the individual ethers, it was recognized that the rates were significantly enhanced in the presence of a few Torr of certain "inert" gases (CO_2, CH_4, N_2, and N_2O), with the gas molecules ultimately serving as guests within the small cages of the CHs, i.e., double CHs of ether−gas molecules were formed. Rate data were therefore determined for formation of EO−CO_2 structure I as well as THF−CO_2 and THF−CH_4 structure II double CHs.

Formation of the double CHs was monitored in the same manner as for the simple ones (above), but in the presence of sufficient CO_2 or CH_4 that pressure change from gas consumption was not a factor. Throughout, the ice particles were prepared from degassed distilled water and reaction was with "Monsanto HP Grade" gases (EO, DME, CO_2, CH_4, and N_2) from which (relatively) noncondensable gases were first removed. The THF-(l) source was Fischer Certified with outgassing.

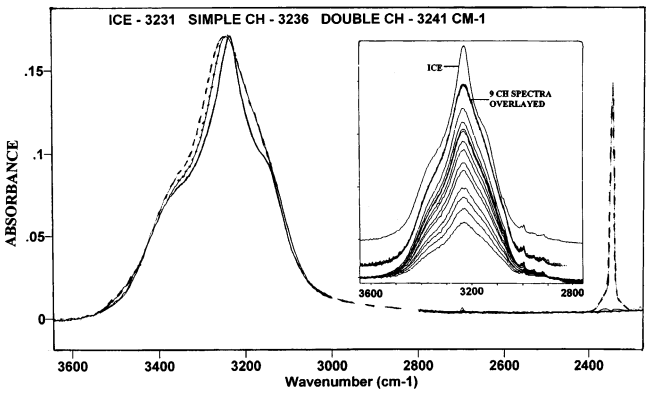

Figure 1. FTIR spectra of the simple (THF) and double (THF and CO_2, dashed line) clathrate hydrates compared with that of an array of ice nanocrystals (solid line). The 2346-cm^{-1} band of CO_2 in the small cage appears on the far right. Stretch bands of the ether, dominated by the embedded ether particles, are omitted. The inset shows the emergence of band intensities of the EO and CO_2 double CH with time (with the ice bands removed). The superposition of the hydrate bands, normalized to the same peak intensity for nine different stages of formation (dark line), indicates the reproducibility of the FTIR difference spectra with the ice components removed.

3. Results and Discussion

The experimental data in each case lead to plots of the fraction of converted ice as a function of time (Figure 2). In the earlier rate measurements, for ice particle conversion to acid hydrates,[16,17] both the nucleation and the basic reaction step leading to acid-hydrate formation were exceptionally rapid. For this reason, in the presence of an abundance of acid adsorbate at the particle surfaces, the much slower rate-controlling process was identified as the transport of the reactant acid molecules to the reaction zone at the interface of the ice core and the growing hydrate crust. Because the crust continually thickens, the transport distance increases monotonically so that the fraction of converted ice (X_b) follows $\sim t^{1/3}$ dependence. For such results, application of the shrinking-core-model equations[26,27] give straight line plots as in Figure 2b, as anticipated for rates controlled by the diffusion of the reactant through product that encrusts the particles. The diffusion constant of the reactant through the crust is then given as $D_e = (\text{slope})\rho R^2/6bC$ where ρ and C are the molar densities of the original particles and the adsorbed reactant, b is the stoichiometric ratio of particle substance to reactant in the product, and R is the particle radius.

An example of a plot of the fraction of ice consumed vs time for HBr dihydrate formation is given in Figure 2a, with comparison made to related plots for ice particle conversion to the clathrate hydrates of EO and DME. The HBr plot is characterized by an initial very rapid reaction rate that quickly decreases as the transport of HBr to the reaction zone becomes rate controlling. By comparison, the DME reaction starts slowly, then increases in rate before ultimately decreasing as diffusion becomes rate controlling. Finally, the EO reaction to form a CH falls between these two extremes of behavior, with a moderate initial rate that decays quickly as the CH crust thickens and EO transport becomes rate controlling.

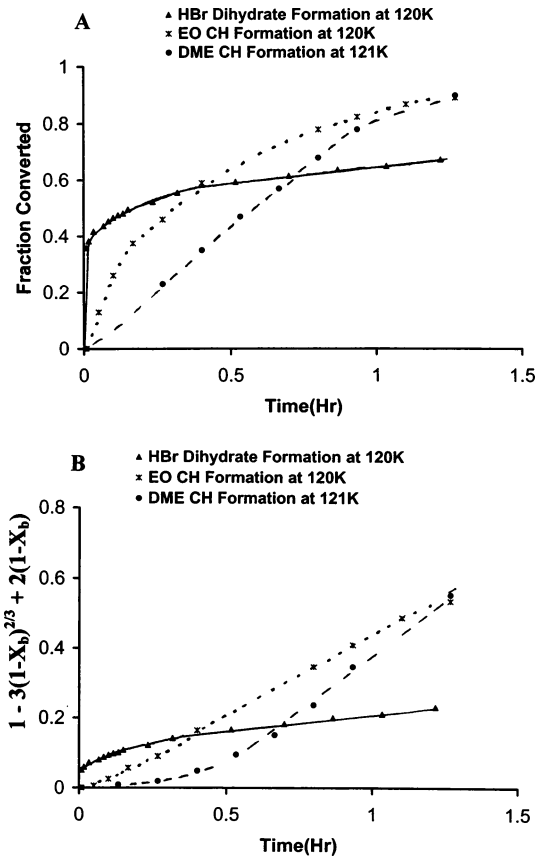

Figure 2. Comparison of typical plots of (A) fraction of ice converted to hydrate vs time for HBr dihydrate, EO clathrate hydrate and DME clathrate hydrate and (B) shrinking-core-model plot of the data of A. The "linear" parts of the latter plots are used to determine D_e. X_b is the fraction of reacted ice for a given exposure time.

The source of this range of behavior becomes clearer when the data are transposed to a shrinking-core plot as in Figure 2b (equivalent to Figure 6 of ref 14). There we see the straight-line behavior for HBr dihydrate formation over a large fraction of reaction time, whereas the induction period for the DME CH appears exaggerated but is ultimately followed by "straight-line" behavior. This does increase the uncertainty in the slope of the straight lines for DME CH formation and, therefore, in the derived D_e value. The induction period of ~0.5 h apparently reflects random nucleation of CH at the surface of the numerous ice particles. The EO reaction induction time is much shorter suggesting a more rapid CH nucleation than with DME. (The initial rapid rate for acid hydrate formation reflects a short period of sufficiently thin hydrate crust that the rate is determined by factors other than transport; i.e., nucleation/inherent reaction rates.)

3.1. Kinetics of Low-Temperature EO CH Formation from Ice Nanocrystals. Data were obtained for numerous kinetic experiments for both the ethylene oxide simple CH and the double CH with CO_2. In both cases the CH is a classic structure I with the large cage populated by the EO. In the absence of CO_2, the EO also populates a small fraction of the small cages, which are filled exclusively by CO_2 in the double CH.

3.1.1. The Simple CH of EO. The earlier studies of CH formation at low temperatures identified EO as the ether capable of forming a CH at the lowest temperature; i.e., ~100 K. It is, therefore, not surprising that ice particle conversion to ether CHs occurs most readily for EO for temperatures near 120 K. Thus we see in Figure 2 that, after a relatively brief induction

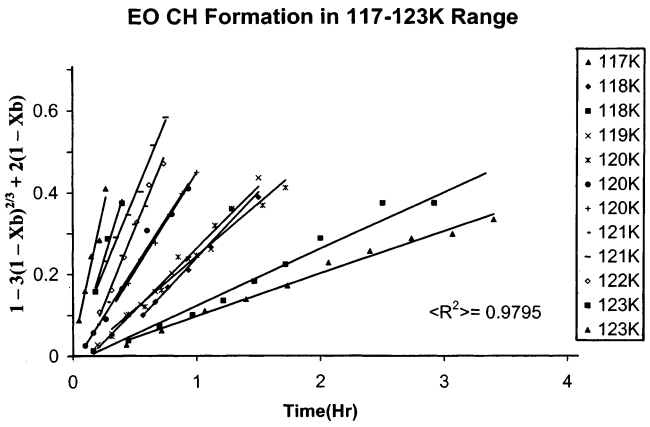

Figure 3. Shrinking-core plots of the rate data for the conversion of ice nanocrystals to nanocrystals of the simple CH of ethylene oxide for the temperature range from 117 to 123 K. X_b is the fraction of reacted ice at a given time.

period, the simple CH of EO forms rapidly at 120 K with the conversion from ice over 80% complete in 1 h. Similar curves for this process have been obtained for temperatures ranging from 117 to 123 K, from which application of the shrinking-core model produced the several straight-line plots of Figure 3 (where X_b is the fraction of converted ice evaluated from FTIR data such as that in Figure 1).

These data plots reveal a significant rate dependence on temperature which the model equation above relates to the temperature dependence of the diffusion coefficient (D_e) for EO within the CH crust that encloses each ice particle.[26] The values of D_e for the simple CH of EO for the ice to CH particle conversions, which range from $\sim 2 \times 10^{-18}$ to 2×10^{-17} cm^2/sec, are tabulated in Table 1. The slope of an Arrhenius plot of these D_e values (Figure 4) indicates an activation energy of 10.6 kcal/mol for EO diffusion within the simple CH. From the concept of low-temperature guest-molecule mobility within ether CHs caused by an unusual concentration of orientational defects (as outlined in section 1), this energy would be related to that required to form/mobilize the orientational defects of the CH. Perhaps significantly it is less by 20−30% than the corresponding value for pure ice.[23,28]

3.1.2. The Double CH of EO and CO_2. Past studies of the (double) CH of EO and CO_2, formed as low-temperature thin films, have shown that the CO_2 occupies the small cages exclusively.[29] Exposure of ice nanocrystals simultaneously to EO and CO_2 similarly lead to a double CH as revealed by the signature small-cage CO_2 band at 2346 cm^{-1} (Figure 1, large cage CO_2 absorbs at 2336 cm^{-1}). Kinetic results for the formation of the double clathrate near 120 K are summarized in Table 1. The simultaneous incorporation of CO_2 into the small cage as the large cages fill with EO has a significant effect on the "EO" diffusional activation energy derived from the rate data as it decreases from 10.7 to 5.0 kcal/mol. Apparently because of this lower activation energy, the ice-to-CH conversion rate is greater by a factor of ~4 in the presence of the CO_2 at 116 K, but the rates converge at higher temperature and (extrapolated) would cross below 130 K. This "CO_2" effect on CH formation rate is relatively small for a given temperature and might be discounted except for a similar much more striking effect in the formation of the double CH with THF (section 3.3.1). The small CO_2 effect on formation rates, relative to the impact in the THF systems, is paralleled by a much smaller CO_2 impact on the O−H stretch-band frequency of the EO CH (Figure 1 vs inset of Figure 1).

TABLE 1: Parameters Determined from Shrinking Core Analysis of CH Formation from ~20 nm (Diameter) Ice Nanocrystals (Values of ρ [moles/mL], C [moles/mL], and b [moles (H_2O)/moles (Guest)] Are Used to Calculate D_e from the Shrinking-Core Equation (Section 3))

medium	D_e (cm^2/s)	Temp (K)	E_a (kcal/mol)
EO CH	1.7×10^{-18}	117	10.6
(simple structure I)	3.8×10^{-18}	118[a]	
$\rho = 0.05$	5.0×10^{-18}	119	
$C = 0.02$	7.8×10^{-18}	120[a]	
$b = 7$	1.3×10^{-17}	121[a]	
	1.2×10^{-17}	122	
	1.9×10^{-17}	123[a]	
EO CO_2 CH[d]	6.8×10^{-18}	114	5.0
(double structure I)	8.3×10^{-18}	115	
$\rho = 0.05$	7.3×10^{-18}	116[a]	
$C = 0.02$	1.5×10^{-17}	118[a]	
$b = 6$	1.9×10^{-17}	119	
	1.6×10^{-17}	120	
DME CH	9.4×10^{-19}	116	14.5
(double structure I)	9.5×10^{-19}	117	
$\rho = 0.05$	3.2×10^{-18}	118	
$C = 0.02$	6.2×10^{-18}	120	
$b = 17$	1.1×10^{-17}	121	
THF CO_2 CH[d]	1.6×10^{-19}	120	10.0
(double structure II)	3.8×10^{-18}	122	
$\rho = 0.05$	6.9×10^{-18}	124[a]	
$C = 0.013$	1.2×10^{-17}	126	
$b = 6$			
THF CH_4 CH[b]	2.4×10^{-18}	118	6.8
(double structure II)	4.2×10^{-18}	120	
$\rho = 0.05$	1.2×10^{-17}	124	
$C = 0.013$	1.4×10^{-17}	126	
$b = 7$			
THF-CH_4 CH[c]	5.8×10^{-18}	118[a]	5.2
(double structure II)	8.5×10^{-18}	120	
$\rho = 0.05$	8.7×10^{-18}	122[a]	
$C = 0.013$	1.7×10^{-17}	124	
$b = 7$	2.5×10^{-17}	126	

[a] Average of 2 values. [b] 5 Torr CH_4 pressure. [c] 10 Torr CH_4 presure. [d] CO_2 equilibrium saturation pressure.

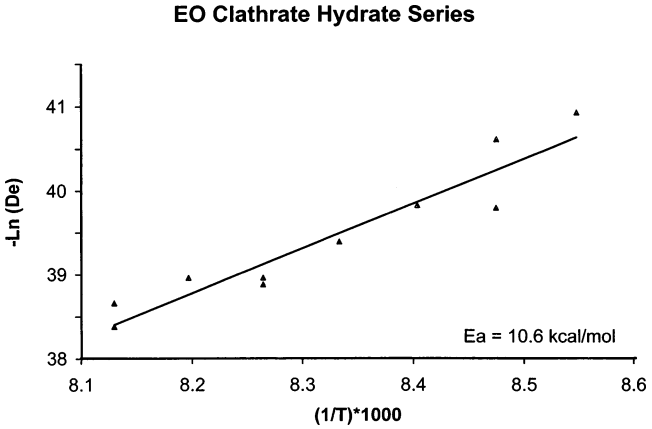

Figure 4. Arrhenius plot of the D_e values (Table 1) for the EO clathrate hydrate as derived from the slope of the Figure 3 shrinking core plots. The D_e values were based on a H_2O:EO stoichiometric ratio of 6 and average nanocrystal diameter of 20 nm.

3.2. Kinetics of Low-Temperature DME CH Formation from Ice Nanocrystals. There is relatively little published information on low-temperature formation of the DME CH, which has been identified as a structure II clathrate.[13] However, reported aspects of the infrared spectra[12] have been confirmed in the present study. The new kinetic measurements indicate formation rates quite similar to those of the EO CH, with one distinct difference that is highlighted in Figure 2. The DME CH seems to nucleate much more slowly than does that of EO, so that nucleation rather than transport controls the rate during early stages of the ice-to-CH conversion. The transport through the hydrate crust does not become the controlling rate factor until significant reaction has occurred. This may reduce somewhat the reliability of the shrinking-core analysis of the formation rates, which was necessarily limited to data obtained after reaction of ~40% of the ice. Because of the slower nucleation of the DME CH, the overall formation times were extended, but the D_e values included in Table 1, determined for ~40−80% ice-to-CH conversion range, were only marginally less than corresponding values for the EO CH. In fact, based on the higher activation energy for transport of DME to the reaction zone (14.5 kcal) the formation rates for DME should surpass those of EO at temperatures several degrees higher than used in this study.

The magnitude of the DME-transport activation energy is surprisingly large, being comparable to the combined formation and mobilization energies of orientational defects in pure ice (~13 kcal[23,28]), which lacks orientational mobility at these temperatures. Clearly, the preexistence of readily mobilized orientational defects cannot fully explain the enhanced CH formation rate. A significant structural influence of encaged DME appears as a strong blue shift of the peak (16 cm^{-1} vs ice, not shown) and the center of intensity of the O−H stretch band. This raises the possibility that, relative to the EO CH, H-bond asymmetry in the DME clathrate hydrate may underlie both the high mobilization energy and an enhanced abundance of the orientational defects induced by the proton acceptor ether molecules. Such H-bond asymmetry is a characteristic of CHs in general, as the oxygen sites divide into three unequal sets with the degree of variation in H-bond lengths dependent on the identity of the guest molecules.[13] It has been suggested that for trimethylene oxide (C_3H_6O), for example, cage distortion by the oversized guest within the structure I clathrate large cages results in sets of H bonds of exceptionally large length differences.[9] As a result, the energy of rotation about H bonds, as required for defect motion, could vary significantly from site to site and thereby frustrate defect mobility. A consequence could be a superabundance of orientational defects (reflecting the weaker-bond population plus the influence of the proton-acceptor ether molecules), offsetting the influence of a high defect mobilization energy. In particular, an elevated defect population could explain an exceptionally large preexponential factor found for the DME diffusion Arrhenius equation. Future kinetic measurements, for formation of the C_3H_6O CH, are planned for comparison of the Ea value with that of DME.

3.3. Kinetics of Low-Temperature THF CH Formation from Ice Nanocrystals. Unlike for EO or DME, exposure of ice nanocrystals to THF vapors near 120 K does not result in a conversion to THF CH nanocrystals on a laboratory time scale. Rather, warming to near 136 K is required to place this process on a time scale of hours. Further, long-term exposure to gases such as CO_2 or CH_4 at temperatures below 160 K, *in the absence of THF*, has no discernible effect on an array of ice nanocrystals beyond the uptake of adsorbate layers on the particle surfaces. However, the combined exposure to an abundance of THF and CO_2 (or CH_4, CO, N_2, or N_2O) near 125 K results in rapid conversion of an ice array to the corresponding double structure II clathrate, but not all gases enhance the enclathration rate of THF. The presence of CF_4, Cl_2, Br_2, or NO did not change the kinetics significantly from that for THF alone. Only data reflecting the "catalytic" influence of CO_2 and CH_4 on enclathration rates of THF are considered here.

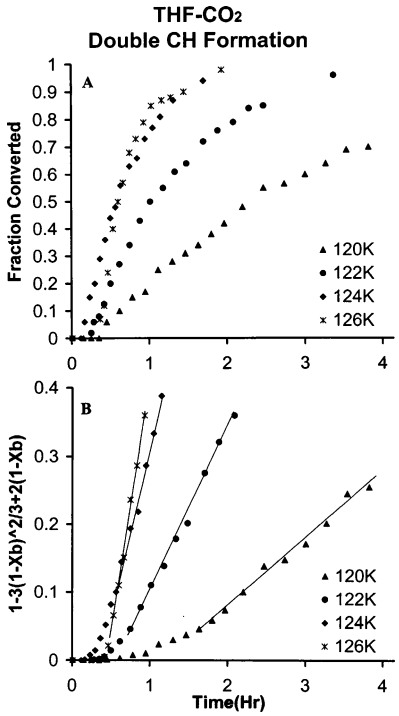

Figure 5. Plots of (A) fraction of ice converted to the double CH of THF and CO_2 vs time for temperatures in the 120−126 K range and (B) shrinking-core-model plot of the data in A. The nearly linear parts of the latter plots are indicated by solid lines. X_b is the fraction of reacted ice at a given time.

3.3.1. CO_2-Enhanced Rates of THF CH Formation. The equilibrium vapor pressure for CO_2(s) at 122 K is ∼0.1 Torr. Ice arrays with interspersed THF nanoparticles, which are inert to CH formation, subsequently show over 80% ice-to-CH conversion when exposed to the equilibrium vapor of CO_2(s) for a 2-h period at 122 K. The plots of Figure 5 show this rapid conversion despite an obvious induction period lasting ∼0.5 h (much as for the case of DME in section 3.2.2). Again, a division of the reaction into two parts, an initial nucleation phase followed by reaction at a rate controlled by guest-molecule transport to the reaction zone, is strongly suggested by the shrinking-core plots of Figure 5b. The straight-line segments, for temperatures ranging from 120 to 126 K, yielded the D_e values of Table 1 for the THF/CO_2 structure II double CH.

The temperature dependence of these D_e values may suggest a 10.0 kcal/mol diffusion activation energy for the guest molecules within the double CH as given in Table 1. However, it is shown in the next section that the CH formation rate for the THF/methane double CH increases with methane pressure. Since the CO_2 saturation pressure increases by a factor of ∼3 over the 6 K sampling range of Figure 5, the 10.0 kcal/mol value should be regarded as an upper limit for the diffusion activation energy.

Since there are two different guest species participating in the growth of the CH crust, the question also arises as to which guest molecules determine the reaction rate as reflected in the value of D_e (and its temperature dependence). In the absence of a molecular model of the formation process there is no clear answer, but both species must play a significant part as the ether is necessary for any low-temperature CH formation, and *the presence of CO_2 accelerates the process by more than 2 orders of magnitude at 126 K*. The presumption of a key role of orientational-defect activity, greatly enhanced by guest-molecule ability to bond transiently with O−H groups of the cage walls (see Introduction), would suggest that somehow THF disruption of the hydrate cage H-bonds is aided by the simultaneous incorporation of CO_2 into the small cages.

A comparison of the O−H stretch spectra of the simple THF clathrate with that of the double CH as given in Figure 1 gives some sign of the influence of the small-cage CO_2 on the bonding of the water network. The water stretch band maximum increases to 3241 cm^{-1} for the double CH from the ice particle value of 3231 cm^{-1}, or roughly twice the blue shift observed for the simple THF CH. This reflects a weakening of some of the H bonds from swelling of the water network structure as a result of occupation of the small cages. (A high small-cage population is apparent from the intense CO_2 band in Figure 1 at 2346 cm^{-1}, the known band frequency for small cage occupancy.[9])

It is reasonable that weakening of the icelike network may facilitate the transient borrowing of O−H bonds from the cage walls by the ether oxygen sites. As described in the Introduction and section 3.2, this might further increase the concentration of orientational defects within the CH, facilitating guest-molecule transport through the crust of CH to the reaction zone. However, this plausible explanation appears inconsistent with similar enhancement of rates by N_2 and CH_4 (section 3.3.2) both of which, being smaller than CO_2, fail to cause a significant blue shift of the hydrate O−H stretch band. Rather, the rate enhancement by methane, accompanied by a much lower D_e activation energy than with CO_2, suggests that the source of catalytic functioning of small-cage guest molecules is varied.

3.3.2. CH_4-Enhanced Rates of THF CH Formation. Methane, like N_2, being more volatile than CO_2, remains largely in the gas phase when admitted to the cold sample cell containing an ice particle array with embedded THF nanocrystals. In fact, at the sampling temperatures near 120 K there is no evidence of CH_4 adsorbed on the ice nanocrystals at CH_4 pressures in the several Torr range. However, with THF nanoparticles present in the array, as a source of abundant THF at the ice particle surfaces, over 90% of the ice is converted to the double clathrate of THF/CH_4 within an hour of exposure to 10 Torr of CH_4(g) at 122 K. The presence of several Torr of methane thus has an effect comparable to that of CO_2 when present at the much lower CO_2(s) equilibrium vapor pressure. This is attested to by the values of D_e for formation of the double CH of THF/CH_4 listed in Table 1. As for CO_2, the presence of CH_4 in the CH small cages was apparent from the FTIR spectra. In particular, a CH_4 bending mode gave rise to a band at 1303 cm^{-1} that sharpened significantly upon cooling to 70 K.

The two sets of D_e values, for temperatures ranging from 118 to 126 K, given for the double CH for two different pressures of CH_4 (i.e., 5 and 10 Torr) show that doubling the methane pressure roughly doubles the enclathration rate. Further, the activation energy for transport to the interfacial reaction zone, which is quite small for the 10 Torr series (5.2 kcal) increases as the methane pressure is reduced. This suggests that the activation energy *for the simple THF CH* at ∼120 K may be significantly larger, a likely reason for no THF enclathration at this temperature in the absence of a "help gas".

4. Summary

The kinetics of a number of systems, in which ice nanocrystals convert to clathrate hydrates of small ether molecules on an hour time scale at ∼120 K, have been investigated by observation of the emergence of the clathrate hydrate spectrum using FTIR difference spectroscopy. At these low temperatures the nucleation of the CH phase of the nanoparticles occurred over a significant time period. This was reflected in an initial

induction period during which the reaction rate increased with time. However, beyond this induction phase the enclathration rate decayed and eventually followed the shrinking- core model of particle reaction indicative of a rate controlled by transport of reactant to an interfacial reaction zone. A close fit of the FTIR spectra at all stages of the reaction to a weighted summation of the ice and CH component spectra provided confirmation of an interfacial solid-state reaction. Therefore, the shrinking-core model was applied to determination of D_e for guest-molecule transport within a growing clathrate hydrate crust and the associated activation energies.

The data also show that the formation of the simple structure I CH of ethylene oxide and structure II CH of dimethyl ether, from ice nanocrystals, occurs on an hour time scale at temperatures as low as 115 K. Further, the formation rates were significantly enhanced and, where examined, the activation energies reduced through simultaneous exposure to small molecules including methane, carbon dioxide, nitrogen, carbon monoxide, and nitrous oxide. The gas molecules participated actively by occupying the small cages of double CHs and thus, from a thermodynamic perspective, would be labeled as "help gases".[13] While temperatures near 135 K were required for similar observations of the formation of the simple structure II CH of THF, the presence of small gas molecules *increased the formation rates by 2 orders of magnitude*. Consequently, the formation rates of the double structure II CHs of THF with methane and carbon dioxide were also determined near 120 K.

There is evidence that rate enhancement occurs only with gas molecules which fit easily within the small cages of the structure I and structure II ether hydrates. The slightly larger molecules CF_4, chlorine, and bromine did not enhance the CH formation rates. However, molecular size is not the only important factor, as the suitably small NO molecule showed little effect on CH formation by THF and did not occupy the small cages of a double CH. This is probably because NO dimerizes when adsorbed on the ice/CH surface. After surface dimerization, which is indicated by a 1768−1864-cm^{-1} doublet of the symmetric−asymmetric N−O stretch modes, the "molecular" size may exceed that for small-cage occupation.

The most interesting aspect of the ether CH formation continues to be the remarkable ability to do so at temperatures at which molecular transport and phase changes in most icelike media are extremely slow. *Formation rates are many orders of magnitude greater than for nonpolar guests* as is particularly clear from comparison of rates reported here with those of ref 14. In the present study, the activity necessary for formation reduces to the transport of the guest molecules to the ice-hydrate interface through the CH crust. The critical aspect of the reaction mechanism therefore becomes that of guest-molecule transport. That mechanism cannot reside in an (unanticipated) exceptional mobility inherent to ether molecules, since in formation of the *double CHs*, small nonpolar molecules also diffuse at comparable speeds to fill the small cages. However, since pure ice particles are inert to nonpolar molecules at 125 K, i.e., no guest transport, the basic mechanism must be based on some special property of ether molecules.

As discussed in the Introduction, the special property of the ether molecules is likely the ability to serve as transient H-bonding proton acceptors (of O−H donated from the cage walls) to generate orientational defects that loosen the network of the host icelike lattice. That is, an elevated population of orientational defects, also evidenced by the remarkably fast dielectric relaxation rates,[13,18,19] serve to "open the cage doors" to allow rapid guest-molecule passage from cage-to-cage and, ultimately, down the gradient within the CH to the interfacial reaction zone. Such defect-facilitated transport would be available to both THF and the nonpolar guest molecules, as observed. The model of the orientational L defects of crystalline ice as presented by Podeszwa, Grishina, and Buch[30−32] includes this conjectured "open door" structure. In fact, the computations of ref 30 show that a typical O···O distance of an L defect in the ice lattice is ∼4 Å, close to the second near-neighbor distance. In a CH, transient rotation of a water molecule to bond to the O-atom of the encaged ether would leave one O···O distance between a pair of water molecules without an intervening H atom, thereby generating an L defect. The resulting cage wall distortion from electrostatic repulsion of the oxygen pair may then provide the "open door" for guest transport. Beyond this conjecture, understanding of the transport mechanism must await detailed molecular-level modeling of molecular diffusion within the CH structures.

Acknowledgment. Support of this research by the National Science Foundation through Grant CHE-0243019 is gratefully acknowledged as are helpful discussions with Prof. Victoria Buch.

References and Notes

(1) Henning, R. W.; Schultz, A. J.; Thieu, V.; Halpern, Y. *J. Phys. Chem. A* **2000**, *104*, 5066.
(2) Wilder, J. W.; Smith, D. H. *J. Phys. Chem. B* **2002**, *106*, 6298.
(3) Mao, W. L. *Science* **2002**, *297*, 2247.
(4) Kuhs, W. F.; Genov, G.; Staykova, D. K.; Hansen, T. *Phys. Chem. Chem. Phys.* **2004**, *6*, 4917.
(5) Circone, S.; Stern, L. A.; Kirby, S. H. *J. Phys. Chem. B* **2004**, *108*, 5747.
(6) Kennett, J. P.; Cannariato, K. G.; Hendy, I. L.; Behl, R. J. *Science* **2000**, *288*, 128. Buffett, B. A. *Annu. Rev. Earth Planet. Sci.* **2000**, *28*, 477.
(7) Ripmeester, J. A.; Ding, L.; Klug, D. D. *J. Phys. Chem.* **1996**, *100*, 13330.
(8) Consani, K.; Pimentel, G. C. *J. Phys. Chem.* **1987**, *91*, 289.
(9) Fleyfel, F.; Devlin, J. P. *J. Phys. Chem.* **1988**, *92*, 631.
(10) Richardson, H. H.; Wooldridge, P. J.; Devlin, J. P. *J. Chem. Phys.* **1985**, *83*, 4387.
(11) Fleyfel, F.; Devlin, J. P. *J. Chem. Phys.* **1990**, *92*, 36.
(12) Hernandez, J.; Uras, N.; Devlin, J. P. *J. Phys. Chem. B* **1998**, *102*, 4526.
(13) Davidson, D. W. Clathrate Hydrates. In *Water, a Comprehensive Treatise*; Franks, F., Ed.; Plenum: New York, 1973; Vol. 2, Chapter 3.
(14) Wang, X.; Schultz, A. J.; Halpern, Y. *J. Phys. Chem. A* **2002**, *106*, 7304.
(15) Uras, N.; Devlin, J. P. *J. Phys. Chem. A* **2000**, *104*, 5770.
(16) Uras-Aytemiz, N.; Joyce, C.; Devlin, J. P. *J. Phys. Chem. A* **2001**, *105*, 10497.
(17) Devlin, J. P.; Gulluru, D. B.; Buch, V. *J. Phys. Chem. B* **2005**, *109*, 3392.
(18) Gough, S. R.; Whalley, E.; Davidson, D. W. *Can. J. Chem.* **1968**, *46*, 1673.
(19) Richardson, H. H.; Wooldridge, P. J.; Devlin, J. P. *J. Phys. Chem.* **1985**, *89*, 3552.
(20) Devlin, J. P. *Int. Rev. Phys. Chem.* **1990**, *9*, 29.
(21) Koga, K.; Tanaka, H. *J. Chem. Phys.* **1996**, *104*, 263.
(22) Wooldridge, P. J.; Richardson, H. H.; Devlin, J. P. *J. Chem. Phys.* **1987**, *87*, 4126.
(23) Wooldridge, P. J.; Devlin, J. P. *J. Chem. Phys.* **1988**, *88*, 3086.
(24) Devlin, J. P.; Buch, V. *J. Phys. Chem.* **1995**, *99*, 16534.
(25) Buch, V.; Bauerecker, S.; Devlin, J. P.; Buck, U.; Kazimirski, J. K. *Int. Rev. Phys. Chem.* **2004**, *23*, 375.
(26) Levenspiel, O. *Chemical Reaction Engineering*; Wiley & Sons: New York, 1962.
(27) Carter, R. E. *J. Chem. Phys.* **1960**, *34*, 2010.
(28) Hobbs, P. V. *Ice Physics*; Clarendon: Oxford, 1974.
(29) Fleyfel, F.; Devlin, J. P. *J. Phys. Chem.* **1991**, *95*, 3811.
(30) Podeszwa, R.; Buch, V. *Phys. Rev. Lett.* **1999**, *83*, 457.
(31) Grishina, N.; Buch, V. *Chem. Phys. Lett.* **2003**, *379*, 418−426.
(32) Devlin, J. P.; Buch, V. Ice Nanocrystals and Ice Adsorbate Interactions: FTIR Spectroscopy and Computer Simulations. In *Water in Confining Geometries*; Buch, V., Devlin, J. P., Eds.; Springer: Berlin, 2003; Chapter 17, p 425.